Direct numerical simulation of three-dimensional swirling n-heptane spray flames

By K. Luo†, H. Pitsch AND M. G. Pai

1. Motivation and objective

Spray combustion is encountered in many engineering applications, such as internal combustion engines and gas-turbine aircraft engines. In these systems, the concurrent processes of liquid atomization, droplet evaporation, turbulent dispersion, and combustion interact and strongly affect each other, which makes experimental measurement and high-fidelity simulation challenging.

To understand these multi-physics phenomena and their strong coupling interactions, methodology of direct numerical simulation (DNS) is helpful. DNS has been proven to be a powerful tool for exploring fundamentals of single-phase turbulent flows (Moin & Mahesh 1998) and turbulent combustion (Vervisch & Poinsot 1998). Recently, DNS has been applied to study spray combustion (Reveillon & Vervisch 2005; Domingo *et al.* 2005; Watanabe *et al.* 2008). Peraa & Reveillon (2007) further applied a two-dimensional compressible solver to explore the spray flame/acoustic interactions. However, all these studies are limited to two-dimensional and simple configurations.

Large eddy simulation (LES) has also been extended to study spray combustion of realistic applications (Moin & Apte 2006; Patela *et al.* 2007). Although consistent results with experimental data have been achieved, using models of gaseous combustion to describe spray flames leads to some modeling issues, as discussed by Baba & Kurose (2008). For example, this approach suggests that combustion can be accurately modeled independent of spray evaporation. However, the combustion process is intricately coupled with the spray evaporation, and combustion models should correctly reflect these interactions.

The present study is motivated by the above background. To gain a better understanding of three-dimensional spray flame behavior, as well as evaporation-combustion interactions in a more realistic configuration, direct numerical simulations of n-heptane spray flames in a model swirling combustor have been conducted. The simulations are performed to approach realistic spray combustion as much as possible. Potential insights into swirling spray combustion are presented, and relevant modeling issues are discussed.

2. Numerical description

2.1. *Flow configuration*

Most previous DNS studies of spray combustion are limited to simple two-dimensional configurations. In the present work, we simulate a more realistic three-dimensional swirling combustor. The geometry of the model combustor is shown in Fig. 1. First, a dimensional

† Current Address: State Key Laboratory of Clean Energy Utilization, Zhejiang University, Hangzhou 310027, P. R. China. E-mail: zjulk@zju.edu.cn

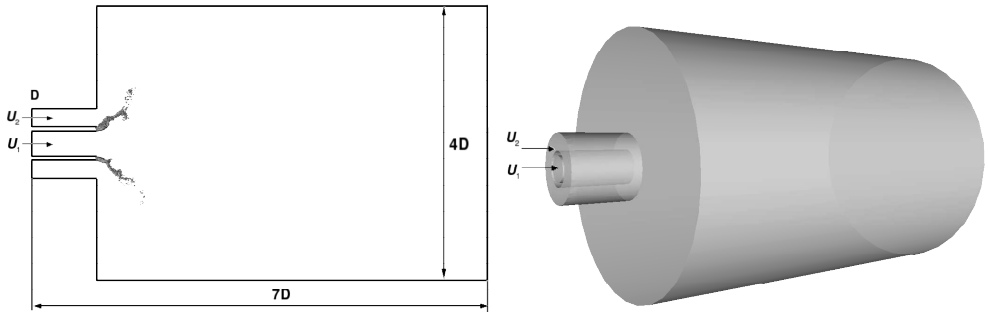

FIGURE 1. Geometry of the present model combustor in two-dimensional and three-dimensional views (left: two-dimensional of the middle azimuthal plane, right: three-dimensional overview).

Swirl number :	$\Pi_1 = \frac{w_g}{u_g} = \mathrm{S}$
Reynolds number :	$\Pi_2 = \frac{\rho_g u_g d_g}{\mu_g} = \mathrm{Re}$
Schmidt number :	$\Pi_3 = \frac{\mu_g}{\rho_g D_g} = \mathrm{Sc}$
Prandtl number :	$\Pi_4 = \frac{\mu_g}{\rho_g a} = \mathrm{Pr}$
Equivalence ratio :	$\Pi_5 = s\frac{\dot{m}_p}{\dot{m}_g} = \Phi$
Stokes number :	$\Pi_6 = \frac{\rho_p d_p^2 u_g}{18\mu_g d_g} = \mathrm{St}$
Spray swirl number :	$\Pi_7 = \frac{w_p}{u_p} = \mathrm{Sp}$
Weber number :	$\Pi_8 = \frac{\rho_g u_g^2 d_p}{\sigma} = \mathrm{We}$
Swirling velocity ratio :	$\Pi_9 = \frac{w_p}{w_g} = \omega$
Density ratio :	$\Pi_{10} = \frac{\rho_p}{\rho_g} = \phi$
Viscosity ratio :	$\Pi_{11} = \frac{\mu_p}{\mu_g} = \gamma$
Temperature ratio :	$\Pi_{12} = \frac{T_p}{T_g} = \kappa$

TABLE 1. Non-dimensional parameters characterizing the swirling spray combustion.

analysis is performed to determine the parameters that characterize the problem. Following standard procedure, the non-dimensional Π terms are obtained after combination and listed in Table 1. To characterize spray combustion in the present swirl combustor, the 12 non-dimensional parameters are necessary. However, some parameters are fixed for a specific air-heptane spray system, such as Sc, Pr, ϕ, γ, and the other parameters are related to boundary or initial conditions. To model a realistic combustor as closely as possible, S, Sp, and κ are chosen the same or close to those in realistic gas-turbine combustors. For simplicity, the Weber number is taken to be small, and the secondary breakup of droplets is not considered. Thus, only Re, Φ, St, and ω are free parameters to be determined in actual simulations. For a DNS study, both Re and St are limited to relatively small values. The remaining parameters, Φ and ω, are varied in the present study to investigate how they influence the spray combustion.

The central swirling air of temperature 500 K is injected through a pipe of inner diameter $D_{\mathrm{in}} = 3.75$ mm with a mean axial velocity $U_{\mathrm{inj}} = 4.5$ m/s and a mean swirl velocity $W_{\mathrm{inj}} = 4.5$ m/s. The secondary swirling air of temperature 500 K is injected

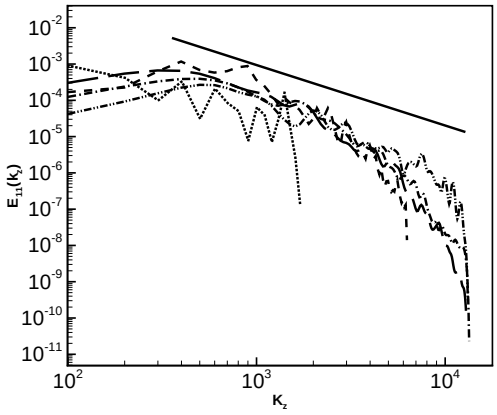

FIGURE 2. Dependence of 1-D axial velocity spectrum on grid numbers: ——— , $k^{-5/3}$; ····· , 192×96×32 (two-phase); – – – – , 384×192×128 (two-phase); — — — , 384×192×256 (two-phase); —·— , 768×384×256 (two-phase); —··— , 768×384×256 (single-phase).

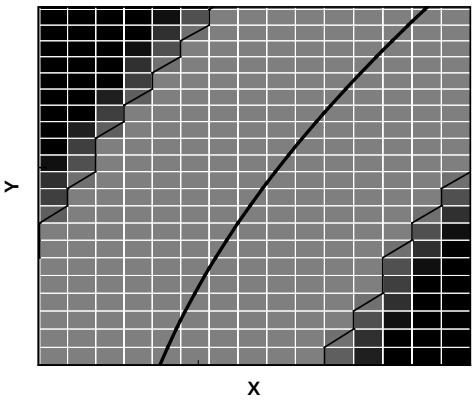

FIGURE 3. Grid distribution across a typical reaction region (solid straight line denotes the stoichiometric mixture fraction position, solid curves represent boundaries of reaction region, and white lines are the underlying grid lines).

through an annular pipe of inner diameter $D_{\rm in} = 5$ mm and outer diameter $D_{\rm out} = 10$ mm with the same mean axial and swirl velocities as those of the central one. This corresponds to a geometric swirl number S=1.0. The combustion chamber is 40 mm wide and 60 mm long, and the outside injection pipe is 10 mm long. The flow Reynolds number based on the mean axial velocity and outer diameter of the pipe is about 3000. The spray is assumed to have been fully atomized, and the resulting n-heptane droplets are issued from the tip of the wall regions between the central and the annular pipes with temperature of 300 K. When the droplets are issued, they are assumed to be in dynamical equilibrium with and have the same velocities as the carrier air. This leads to a spray cone angle of 90^0 and a low Weber number limit. A commonly used log-normal distribution with mean diameter 10 μm, maximum diameter 20 μm, and minimum diameter 1 μm is employed in the present simulations.

2.2. *Grid design*

In DNS of spray combustion, there are strict requirements on the grid resolution. On one hand, the grid size has to be small enough to resolve both the Kolmogorov length scale and the reaction zone thickness of the flame. On the other hand, the grid size has to be around 10 times larger than the droplet size to get correct droplet evaporation dynamics if the point-source assumption of droplets is used, as demonstrated in a previous study (Luo *et al.* 2008). To determine the grid resolution, we perform a grid dependence study. Fig. 2 shows the influence of grid resolution on the one-dimensional axial velocity spectrum. The spectrum is calculated based on the sampled positions in the shear layer region with 10 mm distance to the nozzle and 10 mm distance to the central line for each case. The velocity spectrum becomes independent of grid resolution when 384×192×256 points are used. Considering the resolution requirements for flames, the grid resolution with 768 along the axial direction, 384 along the radial direction, and 256 along the swirling direction is chosen in the present study. In order to capture the important structures as much as possible, the mesh is non-uniform. In the regions of interest, such as the recirculation, strong shear, and near wall regions, finer spacing is used, whereas in other

Case	Equivalence ratio	Swirling pattern	Inflow condition	Reynolds number
A	0.7	Co-swirling	Turbulent inflow	3000
B	0.7	Counter-swirling	Turbulent inflow	3000
C	2.1	Co-swirling	Turbulent inflow	3000
D	2.1	Counter-swirling	Turbulent inflow	3000
E	0.7	Counter-swirling	Bulk inflow	3000
F	0.0	Co-swirling	Turbulent inflow	3000

TABLE 2. Summary of computational cases.

Parameter	Gas turbine combustor	Model combustor
Swirl number	1.0	1.0
Spray cone angle	90°	90°
Schmidt number	0.7	0.7
Prandtl number	0.7	0.7
Damkohler number	O(50)	O(50)
Karlovitz number	O(0.1)	O(0.1)
Droplet-air density ratio	$O(10^3)$	$O(10^3)$
Reynolds number	$O(10^6)$	$O(10^3)$
Swirling velocity ratio	4.0	± 1.0
Droplet Stokes number	$2.5 - 10$	$0.1 - 0.4$
Droplet Weber number	O(50)	O(0.1)

TABLE 3. Comparison of major parameters between realistic gas turbine combustor and the present model combustor.

regions a coarse spacing is used. This clustering is believed to resolve both turbulent scales and chemical scales in the regions of interest, which is demonstrated in Fig. 3 where the typical reaction region extracted from the DNS result is typically resolved by 8 to 10 points.

2.3. *Computational cases*

Different designs for gas turbine propulsion engine combustors have been proposed. Two designs that have been specifically designed to lower NO_x emissions are the so-called Lean Direct Injection (LDI) combustor and the Rich-burn/Quick-quench/Lean-burn (RQL) combustor. To simulate these two cases, the droplet mass flow rate is adjusted to achieve a global equivalence ratio of 0.7 (lean) and 2.1 (rich), respectively. Here, the central and secondary air jets rotate in the same direction (co-swirling). Recent experimental measurements (Hadefa & Lenzeb 2008) show that counter-swirling (flows rotates in opposite directions) imposes different effects on spray combustion. To investigate these effects, lean and rich cases with counter-swirling air jets are also simulated. To further examine the influence of inflow boundary condition on spray combustion, a lean case with a bulk inflow boundary condition is included. Additionally, a single-phase cold flow case is simulated for reference. All these cases are listed in Table 2. To see how the model combustor in the present DNS matches realistic gas turbine combustor, Table 3 gives a comparison of the main parameters used in the DNS and those typically found in realistic engines. The main differences are the flow Reynolds number, droplet Stokes number, and droplet

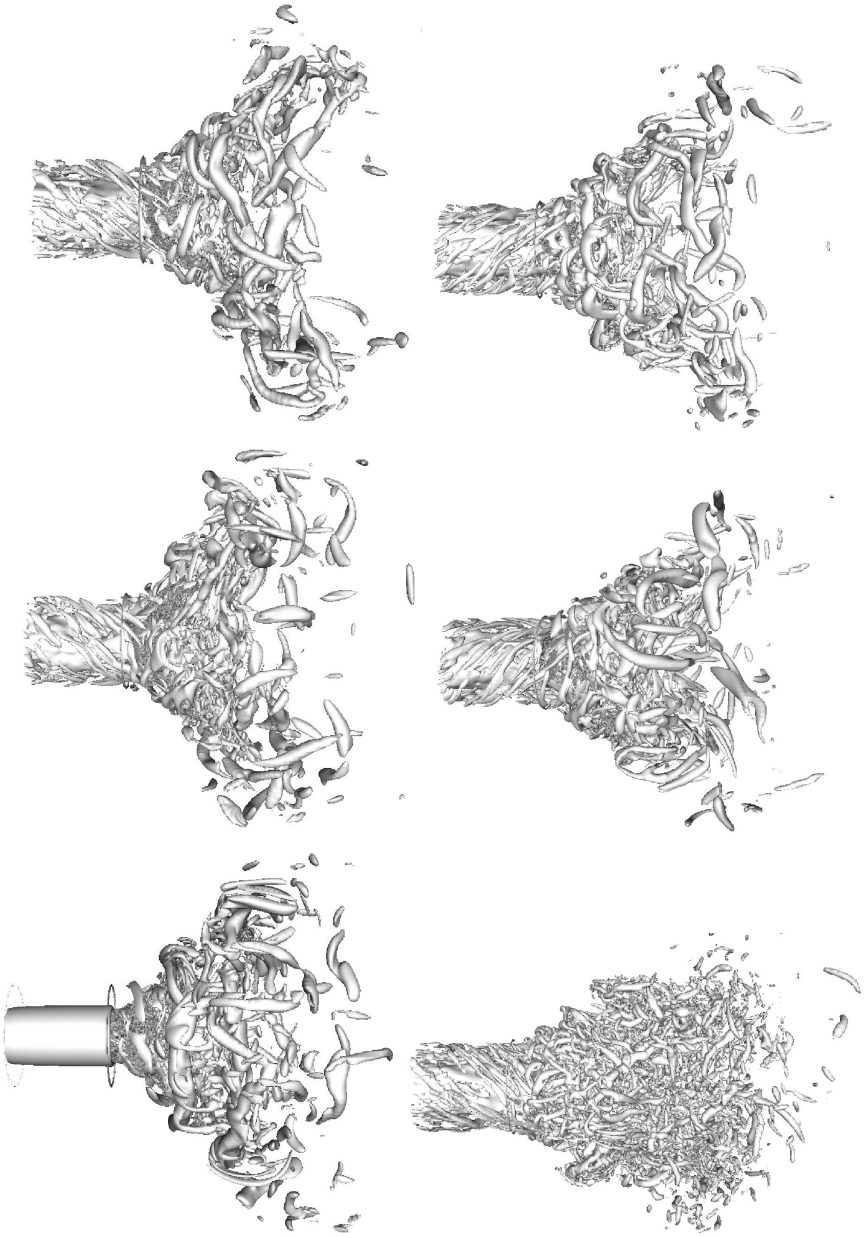

FIGURE 4. Instantaneous vortex structures characterized by Q criterion with same value for different cases (upper left: case A; upper right: case B; middle left: case C; middle right: case D; bottom left: case E; bottom right: case F).

Weber number, all of which demonstrating the limitations of current DNS approach for spray evaporation and reacting flows.

The flow is periodic in the azimuthal direction, and no-slip boundary conditions are used for all walls. The downstream convective outflow condition is obtained by solving a convection equation, allowing for a smooth exit of all structures without perturbing

the rest of the flow significantly. To generate turbulent inflow conditions for the swirling air jets, separate DNS of pipe flows are conducted in the present study, and the data at a certain location are saved and read as the inflow boundary conditions. At first, hot air at a temperature of 1500 K is injected to accelerate the evaporation and trigger combustion. Then the temperature is reduced to 500 K. The data are stored when the flames become approximately stable. Detailed mathematical models, numerical schemes, and model validations for droplet evaporation and combustion have been presented in previous work by Luo *et al.* (2008).

3. Results and discussions

3.1. *Instantaneous vortex structures*

Swirl-stabilized combustion technology has been widely utilized in energy conversion systems. The underlying mechanisms and benefits depend mainly on the formation of large-scale structures in swirling flows, including a central toroidal recirculation zone that recirculates heat and reactive chemical species to the root of the flame and allows flame stabilization and an outer recirculation zone (ORZ). Whereas the formation of the central recirculation zone (CRZ) results from vortex breakdown (Lucca-Negro & O'Doherty 2001), the formation of the outer recirculation zone is related to radial expansion of air stream and wall confinement. Between the CRZ and the ORZ, there are two shear layers, the inner one and the outer one. Although several experimental studies have reported a precessing vortex core (PVC), which is an unsteady vortex located in the inner shear layer precessing around the central axis, in isothermal swirling flows under certain conditions (Midgley *et al.* 2005; Fernandes *et al.* 2006; Cala *et al.* 2006), the occurrence and role of PVC under combustion conditions are still an open issue (Syred 2006).

Fig. 4 compares three-dimensional vortex structures characterized by Q criterion (Dubief & Delcayre 2000) for different cases. In the reacting cases, the vortex structures are mainly the inner shear vortex (ISV) and outer shear vortex (OSV) that originate from the Kelvin-Helmholtz instabilities owing to strong shear in both swirling and axial directions between the CRZ and the ORZ. A recent experimental study (Cala *et al.* 2006) demonstrates that the ISV and OSV appear as helical structures with different helicity signs and hence are counter-rotating. However, the so-called helical dipoles (Okulov & Fukumoto 2004) are not observed, but anti-parallel vortex pairs (Goto & Kida 2003) are observed in the present simulations, even in the bulk inflow case E. This kind of self-organization of structures indicates the inherent tendency of vortex tubes to align themselves anti-parallel in turbulent flows, confirming the previous numerical analysis (Goto & Kida 2003). The self-organized vortex structures in counter-swirling cases are similar to those in the co-swirling cases, but the cone angle is smaller. When compared with the single-phase isothermal case F, obvious differences exist. In the single-phase case, the vortex structures are finer and more numerous. Because the CRZ is not well developed, the cone angle of the structures is smaller. This is also consistent with the previous spectrum comparison in Fig. 2, where droplet evaporation and combustion reduce the spectrum in the high wave-number region.

3.2. *Instantaneous flame structures*

Previous DNS shows that spray combustion is composed of premixed flames and diffusion flames. To visualize the flame structures in the present swirling spray configuration, the normalized flame index (Domingo *et al.* 2005) is used. As seen in the lean co-swirling

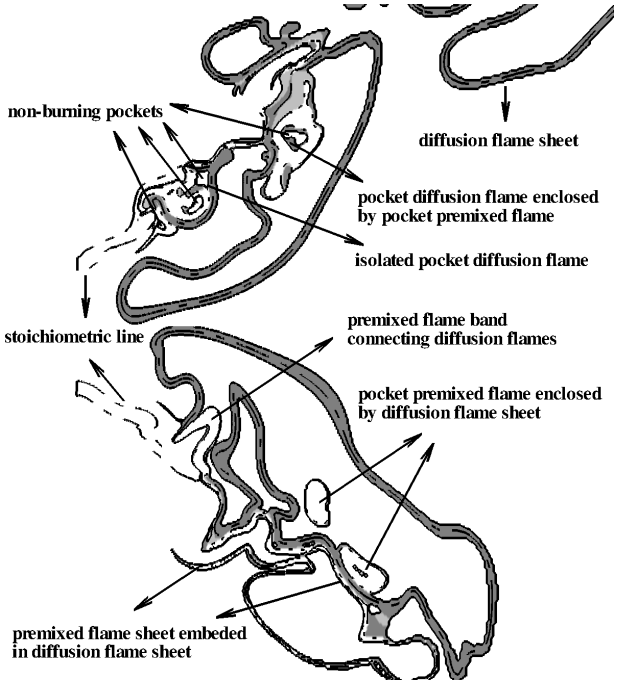

FIGURE 5. Instantaneous spray flame structures in the lean co-swirling case A (—·— : stoichiometric mixture fraction iso-line; ——— : diffusion flame iso-line; —··— : premixed flame iso-line).

case A (see Fig. 5), for example, the spray flame is quite complicated. There are not only isolated diffusion flames and premixed flames, but also their composite structures, for instance, the pocket diffusion flame enclosed by pocket premixed flame, the pocket premixed flame enclosed by diffusion flame sheet, and the premixed flame band connecting diffusion flames. In addition, there are local non-burning pockets in burning flames. All these complex structures are related to the swirling fluid dynamics and turbulent mixing, and bring significant challenges for spray combustion modeling. In particular, the coupled structures always consist of one thick layer and another very thin layer. It is not easy to resolve or model all these thin layers. Generally, it seems that the diffusion flames dominate spray combustion. But in fact, it is premixed combustion that contributes more to the total combustion rate and heat release rate, which will be demonstrated below.

Fig. 5 also indicates that, unlike in pure gaseous combustion, the stoichiometric line in spray combustion is not continuous. Some isolated pocket regions are surrounded by separate stoichiometric lines, suggesting potential local pocket combustion because of a local fuel source of droplet evaporation. However, the local stoichiometric lines certainly do not indicate occurrence of combustion, which is clearly demonstrated close to the nozzle exit. Even for some region at the stoichiometric condition, combustion may not occur due to lower temperature caused by evaporative cooling. Nevertheless, chemical reaction and combustion may also happen in the regions away from stoichiometric composition in a premixed mode. This confirms that the local chemical status cannot be characterized only by the mixture fraction. Other parameters, such as scalar dissipation rate and reaction progress variable, are needed. These parameters have been chosen in flamelet modeling of gaseous combustion (Peters 1984; Pierce & Moin 2004). However,

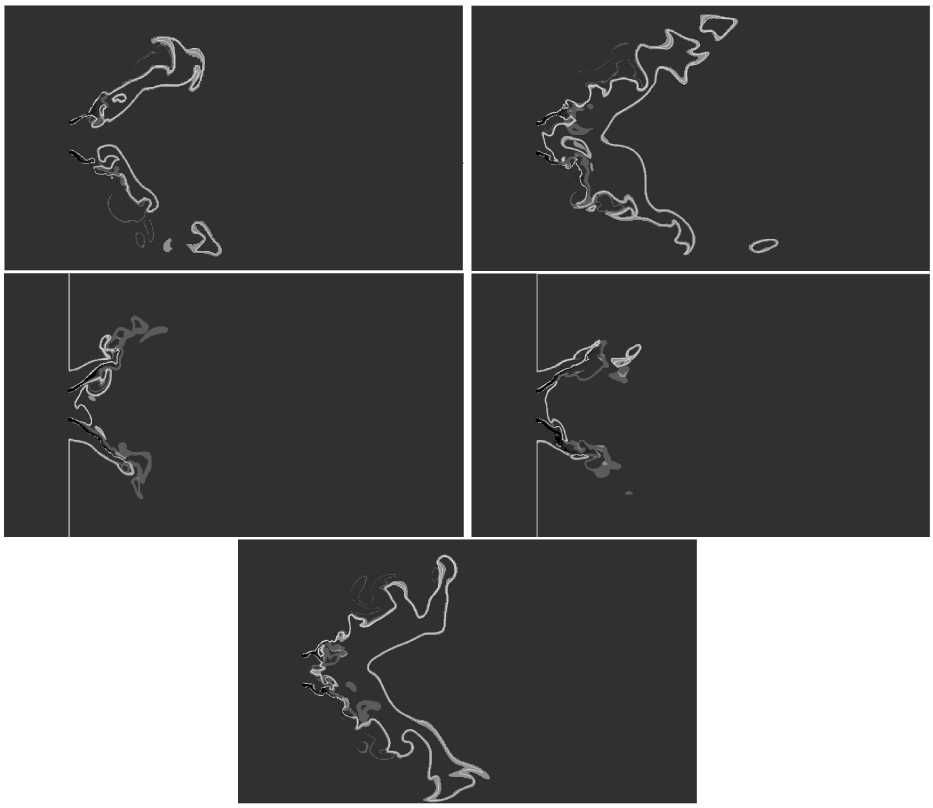

FIGURE 6. Instantaneous droplets superimposed on contour of flame index for different cases (gray denotes premixed flame, and white denotes diffusion flame. upper left: case A; upper right: case B; middle left: case C; middle right: case D; bottom: case E).

it appears that the flame index and droplet evaporation source term potentially serve as additional parameters in flamelet modeling of spray combustion, which will be explored in future studies.

Fig. 6 presents instantaneous contours of flame index for different cases. In the lean cases, most droplets, acting as vapor sources, are separate from the flame front, making spray combustion look more like a pre-vaporization combustion. This could be explained as follows. First, the mean droplet diameter is so small with lean equivalence ratio that it leads to shorter droplet lifetime. Second, the temperature in the evaporation region is reduced even below the inflow air temperature by the evaporation cooling effect, which prevents potential chemical reaction and combustion. Although the evaporation and combustion are almost severed, the evaporation can still influence combustion by altering vapor feeding. By observing the flame topology, the main flame structures are seen as triple flames composed of a rich premixed flame, a diffusion flame, and a lean premixed flame, also some isolated flames. The rich premixed flame lies in the downstream region of droplet evaporation, while the diffusion flame follows the stoichiometric line and is attached by a lean premixed flame branch. Compared with the co-swirling case, the flame structures are more complex in the counter-swirling cases where a diffusion flame forms in the upstream region close to the nozzle exit, and separate diffusion flames become connected to constitute a whole enclosed flame structure in the downstream region. This

indicates that the counter-swirling can enhance turbulent mixing of reactants and make flames more expanded. In both turbulent inflow and bulk inflow conditions, the flame structures in the combustor are similar.

However, both the spray flame structures and the droplet combustion mode substantially change when the global equivalence ratio is increased to 2.1. The droplets have a longer trajectory, but the flame becomes more compact due to the rich condition. A triple flame is also observed, but the locations of component flames are almost in opposite to those in the lean case, i.e., the rich premixed flame forms in the downstream region and the diffusion flame still follows the stoichiometric line but is located upstream, attached by the lean premixed branch in the central region close to the nozzle exit. A diffusion branch also emerges in the central region and connects two premixed branches up and down. As a result, the spray droplets are enclosed by the premixed and diffusion flames, and the typical external group combustion mode forms (Chiu & Liu 1977).

From the flame index, it can also be speculated that the droplet evaporation is mainly driven by the rich premixed flame. Four different stabilization mechanisms for spray flames can be identified. The downstream premixed or diffusion flames are stabilized by the CRZ. The upstream flames located in the shear layer regions are stabilized by the ISV and OSV. The upstream flames attached to the nozzle in the rich cases are stabilized by the nozzle and the ORZ. And the upstream flames located in the central region close to the nozzle are stabilized by the CRZ and nozzle together. These multi-flame patterns and stabilization mechanisms agree with experimental observations from a partially premixed natural gas burner (Vanoverberghe *et al.* 2003). In general, spray combustion is shown to be composed of both lean premixed, rich premixed and diffusion flames under all conditions involved.

3.3. *Conditional mean source terms*

In order to differentiate the roles of premixed and diffusion flames in spray combustion, the conditional mean of evaporation, premixed, and diffusion combustion source terms are defined and calculated as a function of physical coordinates x and y (Luo *et al.* 2008). Fig. 7 presents the distributions of conditional means along axial and radial directions. The heat release has been normalized by its maximum value. It is surprising to find that premixed combustion contributes more than 70% to the total combustion and heat release rate for both lean and rich cases although the diffusion counterpart appears in a wider range. This suggests that more attention should be paid to accurately describe premixed combustion for spray combustion modeling, at least for the present configuration. However, most available spray combustion models rely on only the diffusion combustion model, which should be carefully used according to the present study. Furthermore, the overlap of evaporation and combustion regions indicates that evaporation and combustion are coupled both in time and space. In this condition, the coupling between evaporation and combustion, especially the two-phase mass and thermal coupling need to be correctly handled in any spray combustion model.

3.4. *Unsteady flamelet modeling*

Most diffusion combustion models rely on the scalar dissipation rate to describe the mixing process between fuel and oxidizer. However, the presence of local evaporation modifies the mixing process in spray combustion. The mixture fraction is also no longer

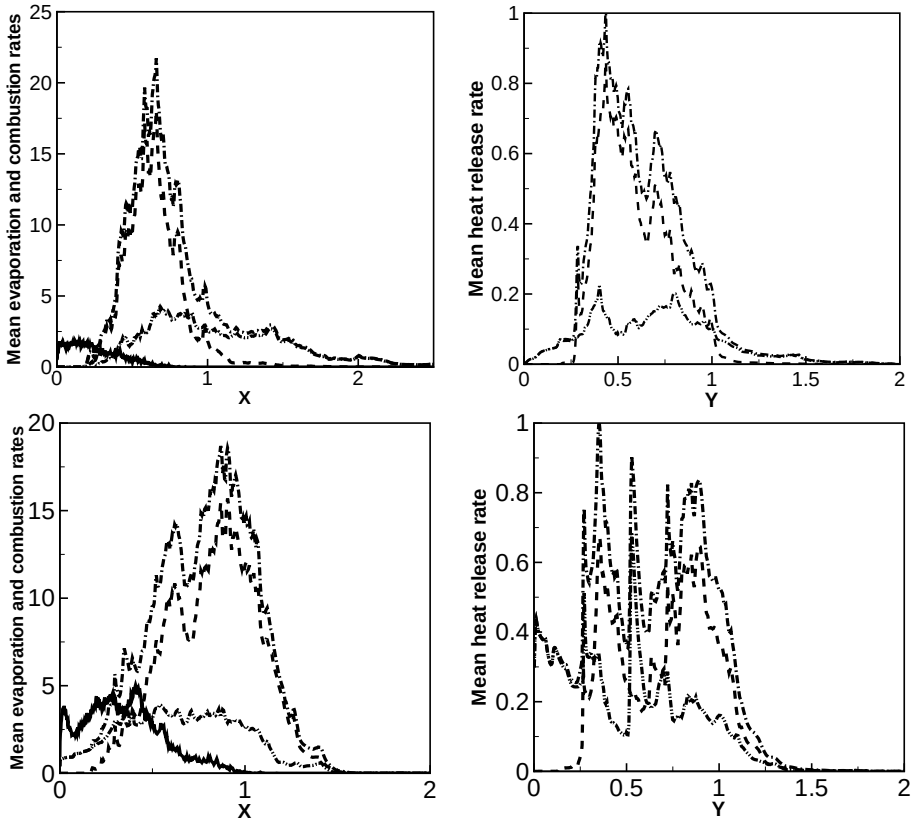

FIGURE 7. Conditional means of evaporation, combustion and heat release rate for cases A (upper) and C (bottom) (——— : evaporation rate; —·—·— : total combustion or heat release rate; – – – – : combustion or heat release from premixed flame; —··—··— : combustion or heat release from diffusion flame).

a conservative variable. Its transport equation can be written as

$$\frac{\partial \rho Z}{\partial t} + \frac{\partial \rho Z u_j}{\partial x_j} = \frac{\partial}{\partial x_j}\left(\rho D \frac{\partial Z}{\partial x_j}\right) + \dot{S}_m. \tag{3.1}$$

Multiplying Eq. (3.1) by the gradient of mixture fraction and using the standard flamelet transformation and assumptions, one can derive an equation for the scalar dissipation rate in mixture fraction space as

$$\frac{\partial \chi}{\partial \tau} + \frac{1}{4}\left(\frac{\partial \chi}{\partial Z}\right)^2 - 2a\chi = \frac{\chi}{2}\frac{\partial^2 \chi}{\partial Z^2} + \frac{2\chi}{\rho}\frac{\partial \dot{S}_m}{\partial Z} - \frac{\partial \chi}{\partial Z}\frac{\dot{S}_m}{\rho}. \tag{3.2}$$

Here τ is the flamelet Lagrangian time that is converted from the axial distance, and a is the rate of strain. Two source terms that involve $\dot{S}_m$ represent the influence of evaporation on the scalar dissipation rate.

To determine if the above equation can correctly describe the affect of evaporation on combustion, Eq. (3.2) is solved with and without the two right-hand side source terms. The evaporation source term $\dot{S}_m$ is extracted from the DNS as a function of the downstream position. The scalar dissipation rate at $x = 0.2$ m is used as an initial condition. The comparisons of the resulting profiles obtained at $x = 0.3$ m with and

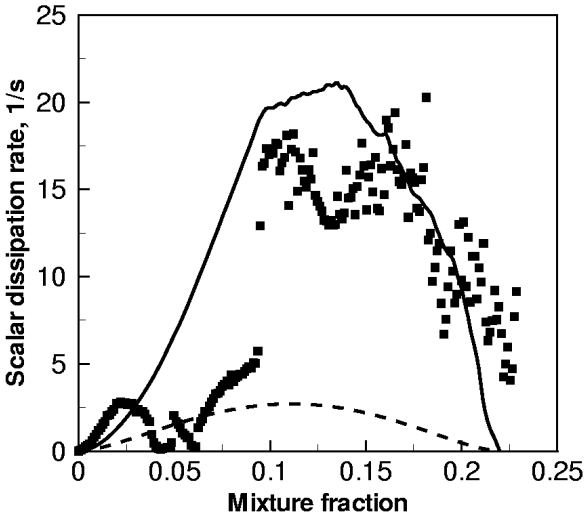

FIGURE 8. Unsteady flamelet modeling for the scalar dissipation rate with different equations (——— : Eq. (3.2) with the two evaporation source terms; – – – – : Eq. (3.2) without the two evaporation source terms; symbol: DNS data at the same axial location).

without the two source terms with the scalar dissipation rate profile extracted from DNS at the same position for the lean case A are shown in Fig. 8. Although some discrepancies exist in the lean side, the equation with the two source terms significantly improves the accuracy compared to the equation without source terms. It suggests that Eq. (3.2) may be used to improve the flamelet modeling of spray combustion, if the two right-hand side source terms are properly represented.

4. Summary and future work

To understand the behavior of realistic spray combustion and interactions of evaporation and combustion, direct numerical simulations of three-dimensional n-heptane spray flames in a model swirling combustor with Reynolds number of 3000 have been conducted. It is found that the spray evaporation and combustion reduce spectrum in the high-wave number region and lead to enlarged CRZ compared with single-phase isothermal case. In addition to CRZ and ORZ which help to preheat reactant mixtures and stabilize flames, ISV and OSV are observed and take on self-organized anti-parallel structures in the simulations. The spray combustion looks more like a pre-vaporization combustion in the lean cases, but changes to external group combustion mode for the rich cases. Although the fluid dynamics, droplet dispersion, and flame structures are subject to different conditions, the swirling spray combustion is stabilized by different mechanism and characterized by lean premixed, rich premixed, and diffusion flames for each case. When evaluating the relative role of premixed and diffusion flames, it is surprised to see that the premixed flames contribute more than the diffusion flames to the total combustion and heat release rate, though their appearance seems to be less. Thus more attention should be paid to correctly describe premixed flame in spray combustion modeling at least for the present kind of configuration. Finally, unsteady flamelet modeling is also developed to account for the influence of evaporation on scalar dissipation rate. Based on

the DNS dataset, relevant issues in spray combustion are being examined. Future issues will examine the presumed scalar dissipation rate profile, PDF of mixture fraction, PDF of progress variable, flamelet equations for spray combustion considering the influence of droplet evaporation, and correlations of evaporation source term and mixture fraction that are usually used in the context of RANS or LES of spray combustion.

Acknowledgments

The authors are grateful to NASA's support of this project. K. Luo appreciates inspiring discussions and help from Professor Parviz Moin, Professor Luc Vervisch, Dr. Olivier Desjardins, Dr. Edward Knudsen, Dr. H. El-Asrag, Dr. Mehdi Raessi, and other colleagues at CTR. Computational resources at Texas Advanced Computing Center (TACC) are acknowledged.

REFERENCES

Baba, Y. & Kurose, R. 2008 Analysis and flamelet modeling for spray combustion. *J. Fluid Mech.* **612**, 45-79

Cala, C. E., Fernandes, E. C., Heitor, M. V., et al. 2006 Coherent structures in unsteady swirling jet flow. *Exp. Fluids* **40**(2),267-276

Chiu, H. H. & Liu, T. M. 1977 Group combustion of liquid droplets. *Combust. Sci. Technol.* **17**, 127-142.

Domingo, P., Vervisch, L. & Reveillon, J. 2005 DNS analysis of partially premixed combustion in spray and gaseous turbulent flame-bases stabilized in hot air. *Combust. Flame* **140**(3), 172-195.

Dubief, Y. & Delcayre, F. 2000 On coherent-vortex identification in turbulence. *J. Turbulence* **1**, 1-22

Fernandes, E. C., Heitor, M. V. & Shtork,S.I. 2006 An analysis of unsteady highly turbulent swirling flow in a model vortex combustor. *Exp. Fluids* **40**(2),177-187

Goto, S. & Kida, S. 2003 Enhanced stretching of material lines by anti-parallel vortex pairs in turbulence. *Fluid Dyn. Res.* **33**,403431

Hadefa, R. & Lenzeb, B. 2008 Effects of co- and counter-swirl on the droplet characteristics in a spray flame. *Chem. Eng. Process* **47**(12), 2209-2217.

Lucca-Negro, O. & O'Doherty, T. 2001 Vortex breakdown: a review. *Progr. Energ. Combust. Sci.* **27**,431-481

Luo, K., Desjardins, O. & Pitsch, H. 2008 DNS of droplet evaporation and combustion in a swirling combustor. *Annual Research Brief*, Center for Turbulence Research, Stanford University/NASA

Midgley, K., Spencer, A.& McGuirk, J.J. 2005 Unsteady flow structures in radial swirler fed fuel injectors. *J. Eng. Gas Turbines Power.* **127**,755764

Moin, P. & Apte, S. 2006 Large-eddy simulation of realistic gas turbine combustors. *AIAA J.* **44**(4), 698-708

Moin, P. & Mahesh, K. 1998 Direct numerical simulation: a tool in turbulence research. *Annu. Rev. Fluid Mech.* **30**, 539-578.

Okulov, V. L.& Fukumoto, Y. 2004 Helical Dipole. *Doklady Phys.* **49**(11),662667

Patela, N., Kirtasa, m., Sankarana, V. & Menon, S. 2007 Simulation of spray

combustion in a lean-direct injection combustor. *Proc. Combust. Inst.* **31**(2), 2327-2334

Peraa, C. & Reveillon, J. 2007 Direct numerical simulation of spray flame/acoustic interactions. *Proc. Combust. Inst.* **31**(2), 2283-2290.

Peters, N. 1984 Laminar diffusion flamelet models in non-premixed turbulent combustion. *Prog. Energ. Combust. Sci.* **10**, 319-339

Pierce, C. D. & Moin, P. 2004 Progress-variable approach for large-eddy simulation of non-premixed turbulent combustion. *J. Fluid Mech.* **504**, 73-97

Reveillon, J. & Vervisch, L. 2005 Analysis of weakly turbulent diluted-spray flames and combustion regimes. *J. Fluid Mech.* **537**, 317-347.

Syred, N. 2006 A review of oscillation mechanisms and the role of the processing vortex core (PVC) in swirl combustion systems. *Prog. Energ. Combust. Sci.* **32**(2),93-161

Vanoverberghe, K. P., Van den Bulck, E. V., Tummers, M. J. & Hubner, W. A. 2003 Multiflame patterns in swirl-driven partially premixed natural gas combustion. *J. Eng. Gas Turbines Power* **125**(1), 40-45

Vervisch, L. & Poinsot, T. 1998 Direct numerical simulation of non-premixed turbulent flames. *Annu. Rev. Fluid Mech.* **30**, 655-691.

Watanabe, H., Kurose, R., Komori, S. & Pitsch, H. 2008 Effects of radiation on spray flame characteristics and soot formation in a counter flow. *Combust. Flame* **152**, 2-13.